



Numerical Simulations of the Monotonic and Cyclic Behaviour of Offshore Wind Turbine Monopile Foundations in Clayey Soils

Mian Xie ¹  and Susana Lopez-Querol ^{2,*} 

¹ University College London, Gower Street, London, UK; mian.xie.18@ucl.ac.uk

² University College London, Gower Street, London, UK; s.lopez-querol@ucl.ac.uk

* Correspondence: s.lopez-querol@ucl.ac.uk

Abstract: Most of the reported centrifuge tests available in the existing literature on offshore wind turbine foundations are focused on the behaviour of monopiles in sands, but very few studies on clayey soils can be found, due to the very long saturation and consolidation periods required to properly conduct experiments in such materials. Moreover, most of the reported numerical simulations using finite element analyses have been validated with monotonic centrifuge tests only. In this research, both monotonic and cyclic performances of offshore wind turbines in clay are validated and justified. The relationship between the monopile rotation in clays and the geometry and strength of the soil has been found and quantified. A prediction of the rotation for a high number of cycles of loading, based on the one experienced by the pile during the first cycle, can be obtained using the correlation derived in the paper. For those cases in which the rotation does not reach a steady value after a high number of cycles, the cumulative rate has been found significantly larger than the prediction conducted with standard analytical methods. A new design methodology for the design of offshore monopile foundations in clay is presented.

Keywords: monopiles in clay; offshore wind turbine foundations; cyclic loading; finite element method; centrifuge tests

Citation: Xie, M.; Lopez-Querol, S. Numerical Simulations of the Monotonic and Cyclic Behaviour of Offshore Wind Turbine Monopile Foundations in Clayey Soils. *J. Mar. Sci. Eng.* **2021**, *1*, 0. <https://doi.org/>

Received:

Accepted:

Published:

Publisher's Note: MDPI stays neutral with regard to jurisdictional claims in published maps and institutional affiliations.

Copyright: © 2021 by the authors. Submitted to *J. Mar. Sci. Eng.* for possible open access publication under the terms and conditions of the Creative Commons Attribution (CC BY) license (<https://creativecommons.org/licenses/by/4.0/>).

1. Introduction

Global warming due to Greenhouse Gas (GHG) emissions is nowadays threatening the economy and living conditions of the world population [1]. The reduction of carbon emissions has become an important issue. The amount of these emissions can be reduced by improving the energy efficiency and developing cleaner alternatives for its production. In December 2015 at the Paris Climate Conference (COP 21), 195 countries agreed that the increment in the global temperature should be controlled within 1.5 degrees centigrade with respect to the temperature at the pre-industrial era [2]. The EU leaders agreed the GHG emissions should be reduced by 5 – 20% compared to the 1990 levels [2]. An energy target was made by the European Union [3] to reduce 40% of the GHG emissions compared to 1990 levels, as well as improving energy efficiency by 27% before 2030. Both the reduction of GHG emissions and the improvement of energy efficiency can be achieved by replacing traditional fossil fuels with renewable energy.

Offshore wind power, one of the cleanest renewable energy forms, has more feasibility than onshore installations due to the lesser required urban planning [4]. As an example, the UK shares about 40% of the wind resources in Europe, and therefore offshore wind power becomes a very feasible approach to reduce GHG emissions in that country [4]. [5] stated that offshore wind power is the most efficient approach to reducing GHG emissions.

Apart from the previously mentioned easier urban planning involved in offshore wind energy production, [6] pointed out that these installations have other advantages, compared to the onshore ones:

- 38 1. the possibility of using large areas allows for major projects, which may introduce
 39 super large turbines, with higher energy production;
 40 2. the offshore wind speed is usually higher than under onshore conditions, which
 41 means that more energy can be generated in a given period (i.e. higher efficiency);
 42 3. less wind turbulence is usually found for offshore conditions; therefore, the energy
 43 can be produced more efficiently and the risk of wind turbine structure fatigue can
 44 be also reduced.

45 Offshore wind farms have a lot of advantages. However, the foundation design of
 46 offshore wind turbines has more uncertainties than for onshore installations. The most
 47 frequent types of offshore wind turbine foundations are sketched in Figure 1.

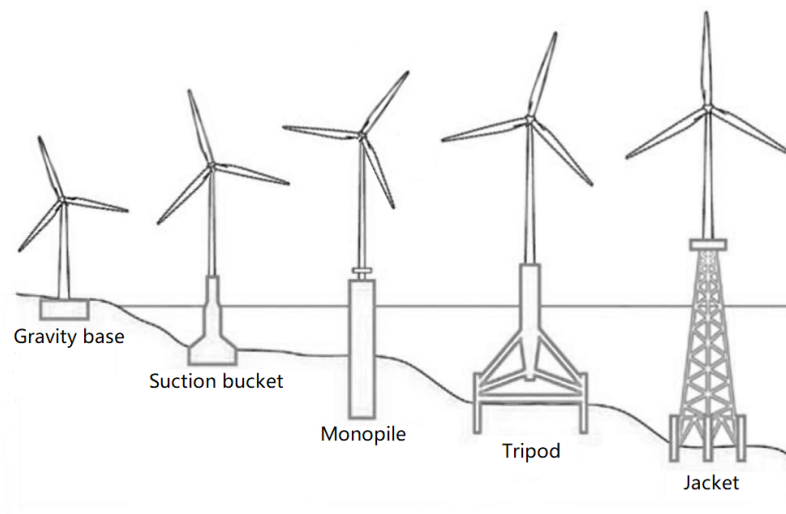


Figure 1. The major types of offshore wind turbine foundation (after [7]).

48 According to relevant industry design guidelines [8], monopile foundations are
 49 usually employed on offshore wind turbines located in shallow waters with a depth of
 50 up to 25m. However, the decision on what type of foundation is to be designed in each
 51 case is usually made based on cost-efficiency and not simply on the water depth. From
 52 the research presented by [9], the monopile foundation is still an economic approach for
 53 water depths up to 35m.

54 In offshore wind turbines, the monopile is a cylindrical hollow steel pile with a
 55 diameter ranging between 3.5 and 7.5m [10]. Monopiles are usually driven into the
 56 seabed with a hydraulic hammer. The length of the pile is about 5 times its diameter (i.e.
 57 ranging between 20 and 37.5m) [11]. The thickness of the monopile can be calculated
 58 according to the pile diameter [12]. Monopiles are currently the most popular offshore
 59 wind turbine foundation due to:

- 60 • easy and fast installation: monopiles can be driven in by a hydraulic hammer and
 61 no prior soil reinforcement is required for the seabed [8];
- 62 • monopiles are easy to manufacture, which is critical for large wind farm projects
 63 that may require the production of hundreds of them [13];
- 64 • the jack-up rig that employed for oil and gas platform foundations can be com-
 65 patible with monopiles; therefore, no special jack-ups are needed for monopile
 66 foundations [13];
- 67 • their analysis and design are relatively simple to undertake due to its regular
 68 geometry and aerodynamic behaviour under loads such as sea waves and wind.
 69 That makes these foundations easy to be modelled.

70 The current offshore wind turbine foundation design is based on the *p-y curves*,
 71 presented in the design guidelines from DNV [8] and API [12]. However, the *p-y*
 72 *curves* in the current guidelines were originally derived from small diameter piles as

73 those employed for gas platform foundations, much smaller than monopile offshore
74 wind turbine foundations. A specific design guideline for large diameter monopiles is
75 not available yet. The behaviour of large and small diameter piles is different: while
76 small diameter piles are flexible, large-diameter monopiles behave more rigidly. The
77 horizontal load applied to a rigid pile tends to overturn it around its toe while flexible
78 piles tend to bend instead. Therefore, applying the current design guidelines to monopile
79 offshore wind turbine foundations usually yields unrealistic estimations and uneconomic
80 solutions.

81 According to the literature, most of the reported centrifuge tests conducted to
82 investigate the behaviour of offshore wind turbine foundations are carried out using
83 sandy soils, and only a few of these studies focused on clays. This is due to the extreme
84 saturation and consolidation periods required to perform experimental research in clayey
85 soils. The number of reported numerical simulations to investigate the performance of
86 monopiles in clays is also very limited. Most of these studies, like those reported by [10]
87 and [14], were only validated using monotonic centrifuge test results, while their cyclic
88 performance is not verified in most cases. However, according to [15], a large number
89 of offshore wind turbine installations in the North Sea are founded in clay, and many
90 newly planned offshore wind farms will also be possibly placed in a clayey area [16].
91 In addition to the research gaps previously stated, the number of finite element studies
92 which concluded with an offshore wind turbine monopile foundation design chart is
93 also limited. This kind of chart allows designers to obtain rapid solutions or checks
94 without running very time consuming full numerical simulations. Additionally, many of
95 the finite element studies on monopile offshore wind turbine foundations reported in the
96 literature lack of detailed explanation of their input parameters, and non-experienced
97 designers may find it hard to implement their own finite element model from the raw
98 laboratory data. Therefore, this research aims to improve the understanding of the
99 non-linear cyclic behaviour of monopiles in clay and contributing to the development
100 of a new optimised monopile design procedure. A design chart will be produced to
101 help the rapid monopile design or checks in clay material, and the employed input
102 parameters will also be presented and discussed in detail. The following stages are used
103 to achieve this aim:

- 104 • establishing a finite element model for offshore wind turbine monopile foundations;
- 105 • validating the model with the corresponding centrifuge test under monotonic loads;
- 106 • validating the finite element model with a centrifuge test under cyclic loads;
- 107 • developing large diameter monopile models based on the previous validations;
- 108 • improving the understanding of the non-linear cyclic behaviour of monopiles in
109 clays;
- 110 • developing a new monopile design procedure based on the numerical simulation
111 results.

112 2. Methodology

113 The simulations conducted in this research have been done using Ansys® Work-
114 bench R18.0 Academic [17].

115 2.1. Model geometry and boundary conditions

116 The numerical simulation of the cyclic behaviour of monopile requires a high
117 computational effort, due to the size, non-linearity and complexity of the problem, as
118 well as the need for time integration procedures to predict the evolution of the system
119 performance in time. As both geometry and loads are symmetric, only half of the
120 problem will be modelled. An example of a symmetric model is shown in Figure 2.

121 The model requires the symmetric boundary condition (symmetry with respect
122 to the yz-plane) to be applied to both pile and soil elements, which means that any
123 displacement in the x-direction for all nodes contained in the symmetry plane will be
124 prevented.

125 In this research, the overall sizes of the model are similar to those reported by [18].
 126 The total horizontal extension of the model is equal to 12D (where D is the diameter
 127 of the pile) and the overall depth of the soil is equal to 1.5L (L denoting the length of
 128 the pile), as depicted in Figure 2. These sizes of the model are proven to generate very
 129 limited boundary effects.

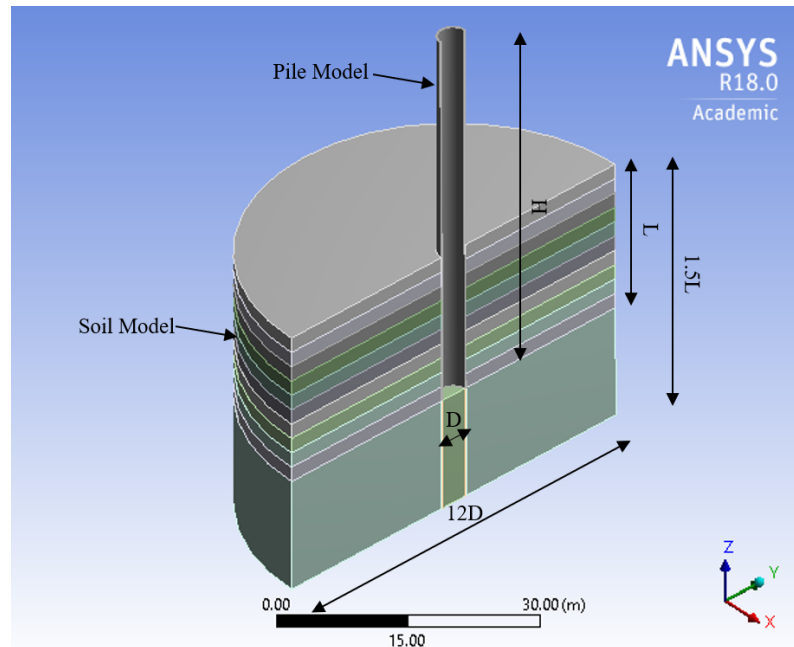


Figure 2. Symmetric model used in this research and its overall dimensions.

130 2.2. Pile modelling

131 The pile was modelled as a hollow solid element. It is assumed as linear, elastic
 132 steel, because it is much stiffer than the soil, and therefore high strains over its yielding
 133 limit are not expected to occur. The pile thickness can be calculated according to the
 134 equation given by the API offshore pile design guidelines of [12], according to which the
 135 pile diameter can be determined as:

$$t_p \geq 6.35 + D/100 \quad (1)$$

136 where t_p is the pile wall thickness (in mm), and D is the diameter of the pile (in mm).

137 The cyclic behaviour of the monopiles with D of 5m, 6.25m and 7.5m have been
 138 modelled. The monopile geometrical properties used to study the cyclic behaviour are
 139 summarised in Table 1, and the properties of the steel used to investigate the cyclic
 140 behaviour of the monopile are those presented in Table 2.

Table 1. Pile geometrical properties.

D - Pile Diameter (m)	t_p - Pile Thickness (mm)	H - Total Pile-structure Length (m)	L - Embedded Length (m)
5.00	57	55	25 - 30
6.25	69	55	25
7.50	82	55	25

Table 2. Pile material properties.

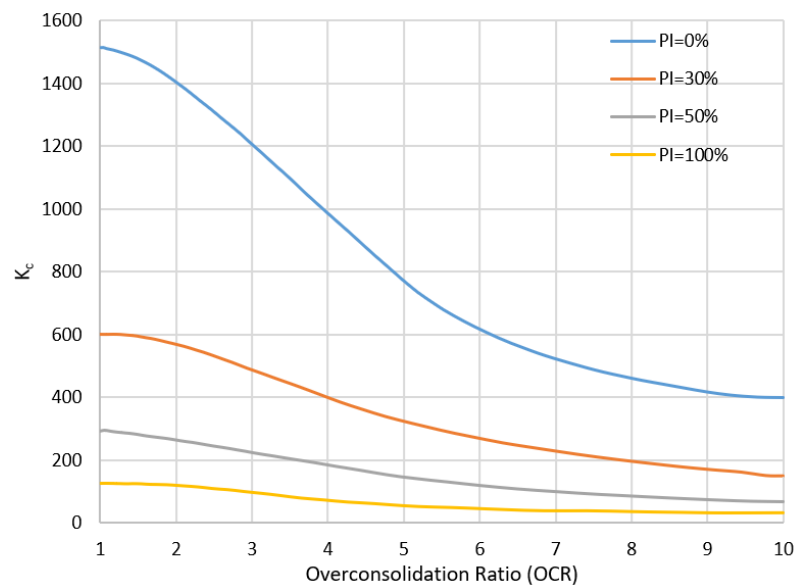
Material	Density (kg/m ³)	Young's Modulus (kPa)	Poisson's Ratio
Steel	7850	200000	0.3

141 2.3. Soil modelling

142 The elasto-plastic Mohr-Coulomb constitutive model requires a very limited set
 143 of parameters, namely: friction angle, cohesion and dilation angle (in addition to the
 144 elastic properties of the soil to simulate its behaviour under the elastic range: Young's
 145 modulus and Poisson's ratio). All these parameters can be very easily determined in
 146 the laboratory, and therefore the uncertainty and the error when the Mohr-Coulomb
 147 model is used mainly comes from the limitation of the model itself rather than from the
 148 uncertainty in its calibration.

149 For saturated clay under undrained conditions, the Poisson's ratio can be assumed
 150 as 0.5. However, to ease the convergence of the numerical simulation, it has been
 151 assumed as 0.495 in the present research. According to [19], the Young's modulus of clay
 152 can be related to the undrained shear strength with a correlation factor K_c , which is a
 153 function of the over-consolidation ratio (OCR) and the plasticity index (PI) of clay, as
 154 shown in Figure 3.

155 For undrained clay behaviour, both friction and dilation angles are negligible. To
 156 avoid numerical instabilities, both angles are taken as small as 1 degree.

**Figure 3.** The relationship between K_c and the over-consolidation ratio (OCR) (after [19]).

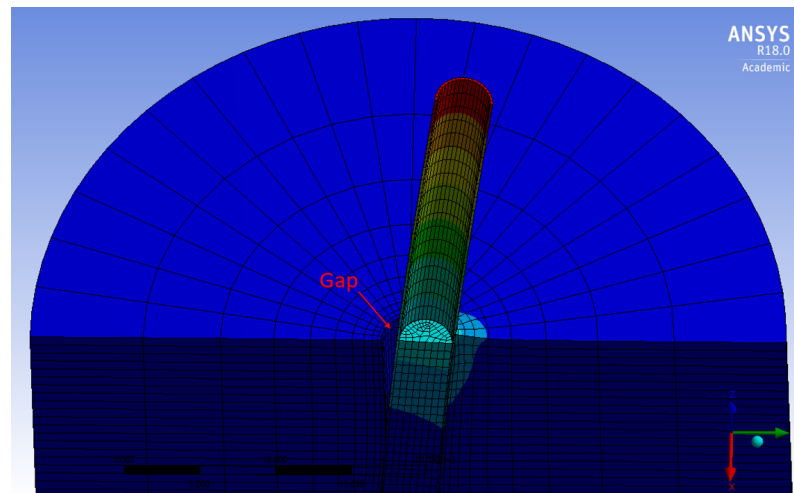
157 The cyclic behaviour of the monopiles in four different clayey profiles has been
 158 investigated. The first three profiles consist of clayey materials reported in [20] (clay
 159 type 1 to 3). The fourth profile analysed consists of layered clay, with two 10m deep
 160 layers of clay types 1 and 2. The properties of the four types of clay used to investigate
 161 the cyclic behaviour of monopile are summarized in Table 3.

Table 3. Soil properties for the cyclic behaviour models (after [20]).

Clay Type	Unit Weight (kN/m ³)	Plasticity Index (%)	Undrained Shear Strength (kPa)	Correction Factor, K _c	Young's Modulus (kPa)
1		44	50	383	19150
2		40	75	447	33525
3	18	38	100	479	47900
4 (0 - 10m depth)		44	50	383	19150
4 (10 - 20m depth)		40	75	447	33525

162 2.4. Soil-pile interface

163 The soil-pile interface was modelled as frictional in this research. The frictional
 164 contact defined in Ansys® allows a gap to be formed between pile and soil, as illustrated
 165 in the example shown in Figure 4. The required input parameter for the frictional contact
 166 is the coefficient of friction. The research on pile-clay interface friction developed by
 167 [21] was used, in which the relationship between the plasticity index and the coefficient
 168 of friction is the one shown in Figure 5, where $\delta_{ultimate}$ and δ_{peak} represent the ultimate
 169 interface friction and peak interface friction angles, respectively. According to [22], δ_{peak}
 170 corresponds to the behaviour of rigid monopiles. Therefore, $\tan \delta_{peak}$ curve shown in
 171 Figure 5 was used to determine the coefficient of friction in this research, through which
 172 for any given plasticity index, the corresponding coefficient of friction can be determined.
 173 The coefficients of friction for each model, obtained from Figure 5, are summarized in
 174 Table 4.

**Figure 4.** Illustration of the formed gap between pile and soil during analysis of lateral load.

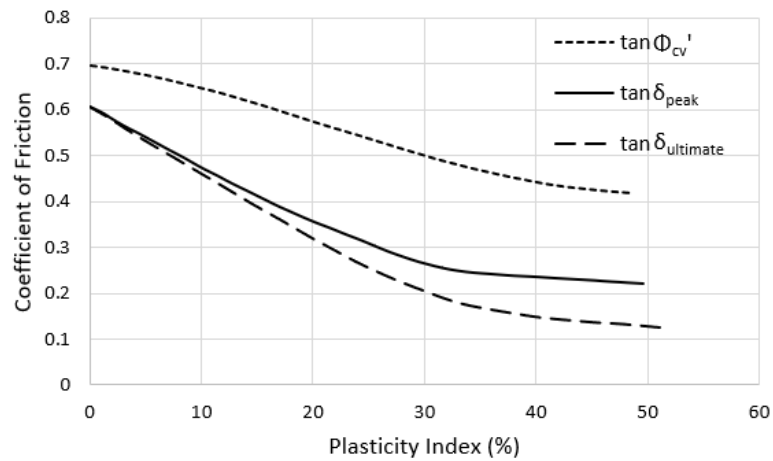


Figure 5. The relationship between the plasticity index and the coefficient of friction (after [21]).

Table 4. Coefficient of friction for each type of clay.

Clay Type	Plasticity Index (%)	Coefficient of Friction
1	44	0.240
2	40	0.247
3	38	0.250
4 (0 - 10m depth)	44	0.240
4 (≥ 10 m depth)	40	0.250

175 2.5. Input loads

176 To reduce the computational effort, the superstructure of the offshore wind turbine
 177 above 30m over the mudline was simplified as a vertical load, representing the weight of
 178 the superstructure and turbine. At this elevation, a punctual horizontal load, assumed
 179 as the resultant force of wind and sea waves, is also applied either statically or cyclically.

180 The typical resultant dynamic load that an offshore wind turbine monopile experi-
 181 ences is of one-way cyclic type, as reported by [18]. Therefore, as in that research, a
 182 one-way cyclic sinusoidal load was used in the present paper to represent the horizontal
 183 load applied to the monopile. A total of 100 cycles were applied to each model, and each
 184 cycle lasted 10s (corresponding to a frequency of 0.1Hz). From [23], the typical peak
 185 vertical and horizontal loads for a 3.5MW offshore wind turbine are 6MN and 4MN
 186 respectively. The peak load represent the combination of critical wave and maximal
 187 wind loads. However, the size of offshore wind turbines has significantly increased
 188 during the last years, and these sizes are expected to keep on increasing in the next future.
 189 Therefore, both vertical and horizontal loads may be doubled for a 5MW offshore wind
 190 turbine, which has a size of about twice larger than those of a 3.5MW one. Therefore, the
 191 peak vertical and horizontal loads applied on the models used to investigate the cyclic
 192 behaviour of monopile have been 12MN and 8MN, respectively. The horizontal load
 193 applied for the cyclic simulation can be described as:

$$F(t) = \text{abs}(F_{max} \sin \pi t / T) \quad (2)$$

194 where *abs* denotes absolute value (one-way load); F_{max} denotes the amplitude of the
 195 horizontal load (8MN in this scenario, for a 5MW turbine); T represents the period of
 196 the load (10s in this case), and t is the time. The loading diagram of the first 10 cycles
 197 is shown in Figure 6.

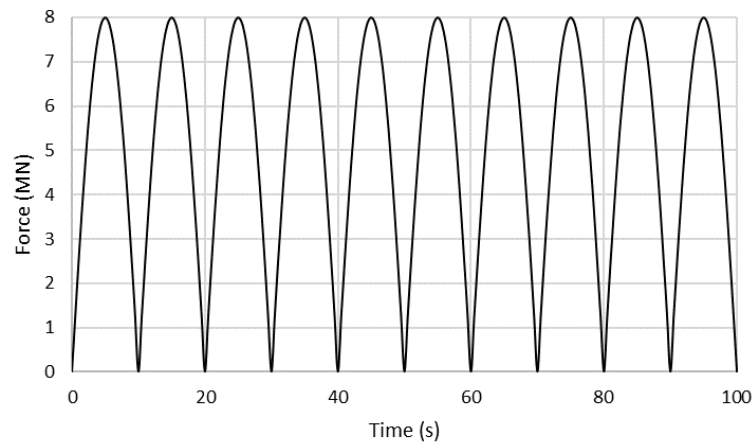


Figure 6. The loading diagram of the first 10 cycles for the 8MN one-way cyclic load.

198 2.6. Mesh density and sensitivity analysis

199 The computational effort is proportional to the mesh density. The coarser possible
 200 mesh density without compromising the accuracy is explored hereinafter. To capture
 201 the pile-soil interaction accurately, the mesh density in the soil domain must be higher
 202 in the proximity of the soil-pile interface. Since a negligible deformation close to the
 203 boundary of the model was found, the mesh density close to these locations was also
 204 coarser. Thus, the mesh density was reduced gradually from the interface to the edges.
 205 The reduced mesh density model resulted in a total of 37405 nodes. [18] found that
 206 accurate results can be generated for the model with 50622 nodes for an offshore wind
 207 turbine monopile foundation problem. In order to investigate the performance of the
 208 reduced mesh density model, a sensitivity analysis on the mesh density was carried
 209 out. A model with a fine mesh resulting in 56932 nodes was running for 10 cycles and
 210 compared with the results achieved with the 37405 nodes model. The mesh reduction in
 211 this analysis is merely applied in the vertical direction as shown in Figure 7 since the
 212 accuracy in the horizontal direction is the most important aspect of this research (because
 213 the input loads are horizontal) and cannot be compromised. Some loss of accuracy due
 214 to the mesh reduction in the vertical direction can be assumed though. Both meshes are
 215 shown in Figure 7.

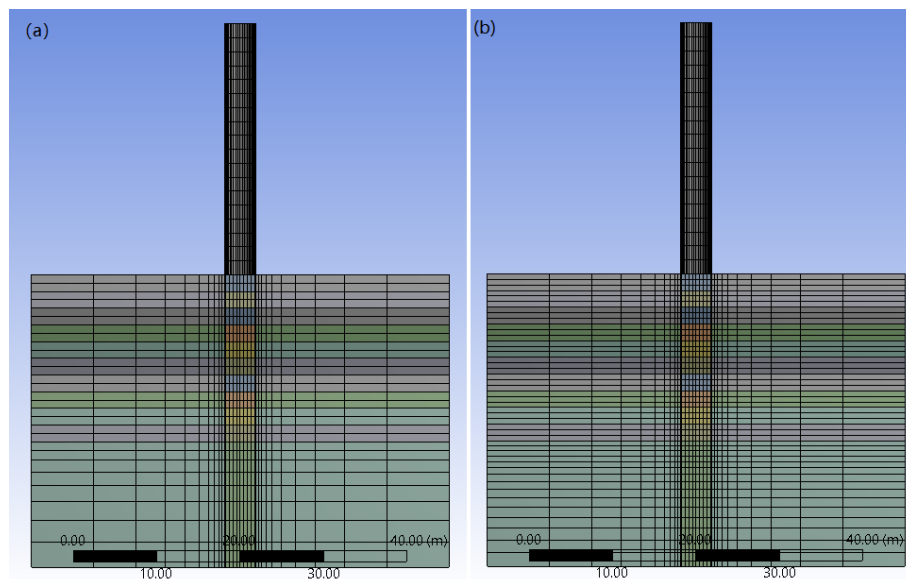


Figure 7. Mesh density, (a) 37405 nodes model. (b) 56932 nodes model.

216 The time history of the pile head displacement has been plotted in Figure 8, where
 217 it can be seen how the reduced mesh density model slightly over-estimates the pile
 218 head displacement. However, the results generated with the coarser model are close
 219 enough to those of the denser model, and therefore the accuracy of the solutions is not
 220 significantly compromised with it, while the efficiency highly increases. Therefore, the
 221 coarser mesh is employed in the simulations presented hereinafter.

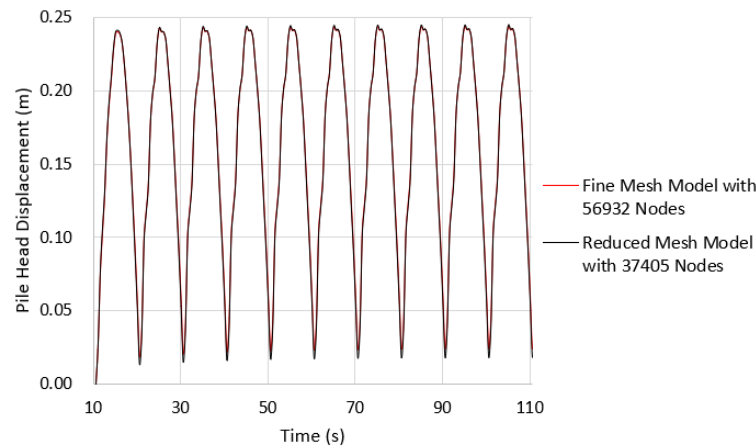


Figure 8. Time history of the pile head displacement in the sensitivity analysis.

222 3. Validation of the numerical model

223 3.1. Centrifuge tests

224 Both monotonic and cyclic numerical models have been validated using the cen-
 225 trifuge tests results obtained by [16], who report results out of 1000 cycles of loading.
 226 Those tests were conducted on large diameter monopiles (dislike other cases on small
 227 diameter of rigid piles like those carried out by [24] and [25], among others). In this
 228 section, these centrifuge tests are described and discussed.

229 [16] investigated two pile geometries with pile diameters of 3.83 and 7.62m in five
 230 different soil profiles. A total of nine centrifuge tests were carried, namely, test numbers
 231 OWF-01 to OWF-09. Figure 9 shows the setup for the centrifuge tests. The embedded
 232 length of the pile was 20m, and the force was applied 30 m above the mudline. The
 233 vertical force applied was 6MN for the 3.83m diameter pile and 12MN for the 7.62m
 234 diameter pile. Table 5 summarises the five different site conditions, while Table 6 shows
 235 the summary of these nine tests.

236 Tests OWF-01 to OWF-03 (Phase I) were monotonic experiments with 3.83m diam-
 237 eter piles on the prototype scale. Moreover, tests OWF-04 to OWF-08 (Phase II) were
 238 cyclic analyses with 3.83m diameter piles on the prototype scale. Test OWF-09 (Phase
 239 III) was a cyclic test with a 7.62m diameter pile on the prototype scale.

240 The cyclic tests (OWF-04 to OWF-09) were subdivided into seven stages based
 241 on their loading patterns, as shown in Table 7 [16]. In general, the tests in stages 1, 2
 242 and 5 were subjected to one-way cyclic loading. The tests in stage 7 were subjected to
 243 monotonic push. Either 1-way or 1.25-way cyclic loading is applied in the rest of the
 244 stages. From stages 1 to 6, the test with a higher stage number has a larger peak load.

245 Tests OWF-03 and OWF-09-stage-4 have been selected in the present paper to
 246 validate monotonic and cyclic numerical models, respectively. The rationale behind this
 247 selection was to choose the centrifuge tests with potentially lowest uncertainty within
 248 their categories (i.e. monotonic and cyclic). The experiment results obtained for OWF-03
 249 may have lower uncertainty than the other two monotonic tests (i.e. OWF-01 and OWF-
 250 02) because it was the last monotonic test conducted, which means that the experiment
 251 operator [16] has developed sufficient experience and skills from the previous runs
 252 OWF-01 and OWF-02. Therefore, OWF-03 is selected for the validation of the monotonic
 253 numerical model.

254 As previously described, the cyclic tests reported by [16] are subdivided into several
 255 stages based on the loading profiles. The initial aim of that research was to conduct
 256 1-way and 1.6-way cyclic loading rather than 1-way and 1.25-way because the monopile
 257 has the highest response (accumulated rotation) under 1.6-way load. However, this
 258 plan was abandoned because of the unaccepted experiment error [16], implying that
 259 the monopiles which had higher responses during the experiments may also have more
 260 uncertainty in their solutions. On the contrary, those monopiles which experienced
 261 an extremely low response may be associated with considerable uncertainty as well.
 262 For example, the experiment results from Stage 1 have not been documented by [16],
 263 possibly because the peak loads in stage 1 (3 and 6kN) were not high enough to develop
 264 the non-linear soil behaviour. Although the results are documented for stage 2, the
 265 highly dispersed data points shown in this stage seem to indicate high uncertainties.
 266 Therefore, the tests subjected to moderate peak loads seem more reliable. Those tests
 267 are on stages 3 and 4. One source of uncertainty given by loads application during the
 268 experiments can be quantified by exploring Table 7, where the ideal minimum load
 269 should be zero for the 1-way scenario and 0.25 times its maximum load, for the 1.25-
 270 way scenario. Therefore, the uncertainty can be simply calculated by the difference
 271 between actual and ideal minimum loads divided by the peak load. From Table 7 and
 272 the application of the proposed uncertainty calculations, OWF-06-stage-4 and OWF-07-
 273 stage-4 have the lowest uncertainty, which is 0% and 1%, respectively. Furthermore, [16]
 274 disclosed that OWF-06 and OWF-09 might have larger uncertainties because of reported
 275 inappropriate operations. Therefore, the OWF-07-stage-4 is adopted as the one with the
 276 lowest uncertainty in these cyclic tests.

277 The material used in the test was Kaolin, and the triaxial test conducted for this
 278 clayey material, along with its main soil properties (such as specific gravity and
 279 plasticity index), are documented by [16]. Besides the triaxial test, the over-consolidation
 280 ratio and the undrained shear strength profile along with the depth were measured
 281 during the tests.

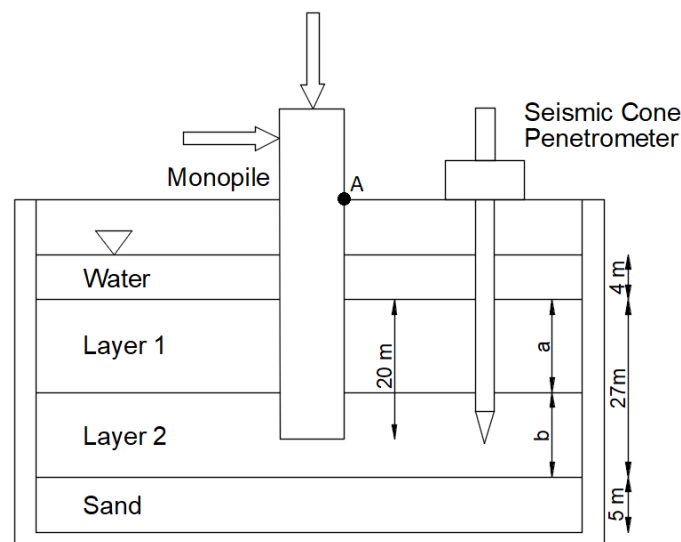


Figure 9. Setup for the centrifuge test (after [16]).

Table 5. Five site conditions used in the test (after [16])

Site	Layer 1		Layer 2	
	Depth a (m)	Consolidation Pressure (kPa)	Depth b (m)	Consolidation Pressure (kPa)
A	13.5	500	13.5	500
B	13.5	300	13.5	300
C	13.5	180	13.5	180
D	5.0	180	22.0	500
E	10.0	180	17.0	500

Table 6. Experimental programme on the prototype scale (after [16]).

Phase	Test Number	Test Nature	Pile Diameter (m)	Vertical Load (MN)	Site Specification
I	OWF-01	Monotonic	3.83	6.5	B
	OWF-02			6.5	A
	OWF-03			4.0	C
II	OWF-04	Cyclic	7.62	4.0	C
	OWF-05			6.5	B
	OWF-06			6.1	A
	OWF-07			6.0	D
	OWF-08			6.1	E
III	OWF-09	Cyclic	7.62	12.0	A

Table 7. Stages and loading profiles for OWF-06 to OWF-09 (after [16]).

Stage	OWF-06		OWF-07		OWF-08		OWF-09	
	Min, Max Load (N)	No. of Cycles	Min, Max Load (N)	No. of Cycles	Min, Max Load (N)	No. of Cycles	Min, Max Load (N)	No. of Cycles
1	0, 3	1000	0, 3	1000	0, 3	1000	0, 6	1000
2	-3.2, 36	1000	2, 32.5	1000	0.2, 31.2	1000	-1, 60	1000
3	-2.5, 79	1000	-19.5, 56.5	500	3.6, 79	1000	5, 150	1000
4	0, 100	100	-0.6, 100	500	10.6, 111	500	17.3, 223	1000
5	NA	NA	-30, 123	479	-30.6, 121	500	-65, 238	500
6	NA	NA	14, 167.5	500	-12.5, 140	500	-86, 217	500
7	Monotonic Push							

282 3.2. Input parameters and results of the validations

283 To closely represent the real soil conditions during the tests, the soil profile was
 284 sub-divided into 11 layers in the model as shown in Figure 10. The top 20 meters of
 285 soil where the pile was embedded were divided into 10 layers, 2m deep for each one
 286 of them. The soil beneath the pile was modelled as a single layer since no significant
 287 soil-pile interaction was expected at this location.

288 The soil properties reported by [16] (plasticity index, the over-consolidation ratio
 289 and the undrained shear strength profile along with the depth) are employed in the
 290 numerical simulations. The Kaolin clay employed in these tests had a plasticity index
 291 equal to 33%. As both the plasticity index and the OCR are known, the correction
 292 factor K_c for each layer can be obtained from Figure 3. Therefore, the Young's modulus
 293 (E_s) for each layer can be calculated by the correction factor (K_c) multiplied by the

294 undrained shear strength (C_u) in each layer. The input soil properties for each layer are
 295 presented in Table 8. According to [16], centrifuge tests OWF-03 (used for validating the
 296 monotonic behaviour) and OWF-07-stage-4 (used for validating the cyclic behaviour)
 297 were conducted using different soils, the properties of which are summarized in Table 8.
 298 Layer 1 is the surface soil layer, while layer 11 is the bottom one.

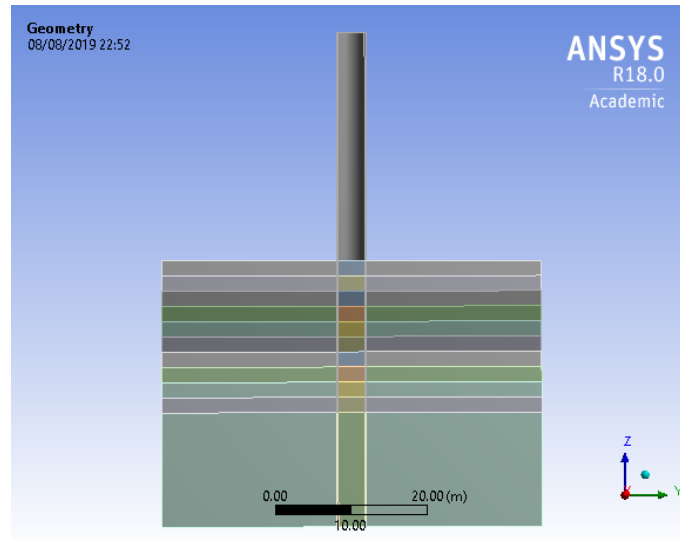


Figure 10. Model with 11 layers of soil, used for validation with the centrifuge test.

Table 8. Input soil properties for validating the monotonic and cyclic behaviour (after [16]).

Layer	Depth (m)	Monotonic Behaviour Validation				Cyclic Behaviour Validation			
		OCR	K_c	C_u (kPa)	E (kPa)	OCR	K_c	C_u (kPa)	E (kPa)
1	1	14.7	147.0	7.7	1126.4	14.7	147.0	24.0	3520.8
2	3	9.8	152.6	12.3	1879.2	9.8	152.6	27.1	4137.3
3	5	5.8	278.3	14.4	3998.4	5.8	278.3	35.9	9999.7
4	7	4.0	397.0	15.9	6301.1	10.4	147.0	44.6	6547.5
5	9	3.1	483.0	17.2	8326.7	8.0	197.7	46.9	9264.0
6	11	2.5	527.7	18.1	9530.9	6.5	251.0	50.2	12607.2
7	13	2.1	561.7	18.6	10453.4	5.5	293.0	54.4	15948.2
8	15	1.8	579.6	19.2	11103.3	4.7	341.0	56.3	19205.9
9	17	1.6	589.2	19.7	11608.8	4.0	394.0	60.9	24012.6
10	19	1.3	597.3	21.2	12668.1	3.5	441.0	65.4	28823.3
11	20	1.3	599.5	22.0	13206.5	3.3	454.0	67.9	30817.9

299 The pile geometry and the applied loads were exactly the same as for the prototype
 300 scale in the centrifuge test: $D=3.83\text{m}$, $t_p=1.67\text{mm}$ and $L=20\text{m}$. The coefficient of friction
 301 between pile and soil can be obtained from Figure 5, taken as 0.250 for the 33% plasticity
 302 index.

303 According to the centrifuge test conducted by [16], the monotonic pushover was
 304 displacement-controlled. The reaction force at the pile head and the mudline displacement
 305 were measured during the centrifuge test [16]. The mudline displacement was
 306 measured at point A as shown in Figure 9. Figure 11 shows the validation for the
 307 monotonic model. Despite some instability observed in the experimental results, probably
 308 due to inaccuracy of the transducers, it can be seen that the agreement between
 309 numerical and experimental results is excellent. From this analysis, it can be concluded
 310 that the Mohr-Coulomb constitutive model is reliable enough to describe the monotonic
 311 behaviour of monopiles in clay. From the figure, it can also be seen that the numerical

simulation slightly over-estimates the initial horizontal displacement which is consistent with previous results, reported by [10] and [14].

[16] documented the cyclic behaviour of the monopiles as the cumulative rotation for the pile at the mudline. Same as [16] and [11], in this paper the cumulative rotation for each cycle has been normalized with respect to the rotation of the first cycle. The results obtained from this centrifuge test are presented in Figure 12. Moreover, [16] reported a comparison between their experimental results and a prediction with the methodology proposed by [11], also plotted in Figure 12. The results obtained with the numerical model developed in the present research are also included in Figure 12, showing a much better agreement when compared with the experimental results. From this comparison, it can be concluded that the Mohr-Coulomb constitutive model can be considered accurate enough to describe the pseudo cyclic behaviour (cumulative rate of rotation) of monopiles in clay. It should be noticed that only the cumulative rate of rotation (ϑ_N/ϑ_0) can be validated; the force-displacement hysteresis loops cannot be validated by the centrifuge test due to the well-known limitation of Mohr-Coulomb constitutive model. This is the reason why it is called pseudo cyclic behaviour (i.e. the cumulative rate of rotation is true, but the force-displacement hysteresis is pseudo). Therefore, the following analyses, based on Mohr-Coulomb model, are merely focused on the pile rotation in the first cycle (monotonic behaviour) and its cumulative rate of rotation.

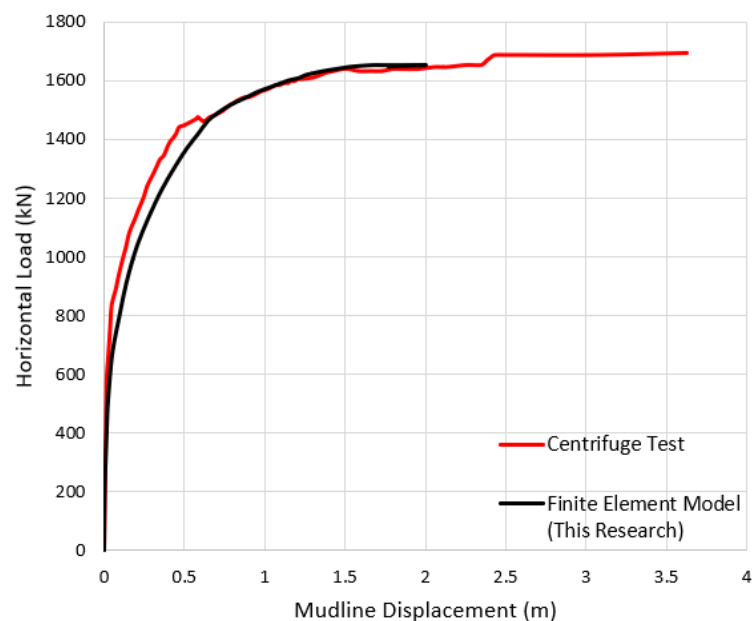


Figure 11. Validation of the monotonic model.

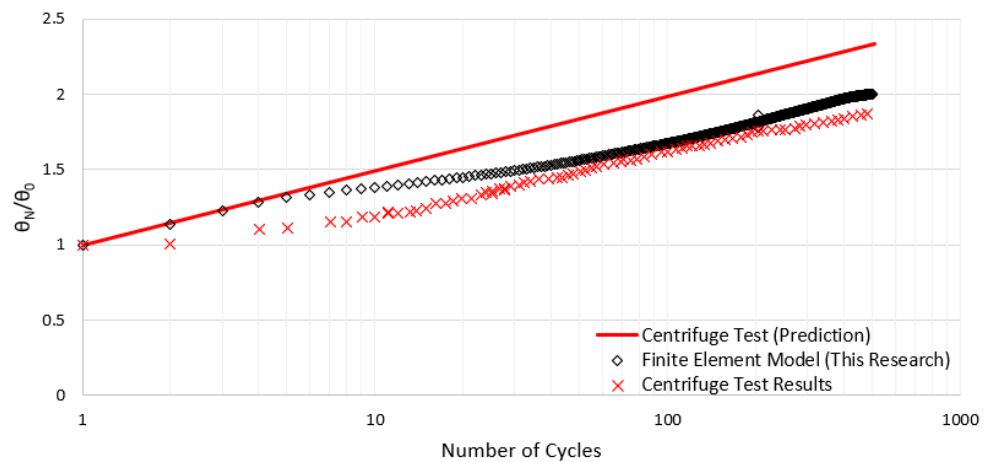


Figure 12. Validation of the cyclic model.

332 4. Results

333 Once both monotonic and cyclic models have been validated, a set of simulations
 334 has been conducted to investigate the cyclic behaviour of monopiles with different
 335 geometries and types of clay. Three piles, with a diameters, D , of 5, 6.25 and 7.5m, have
 336 been modelled, using three types of clay with undrained shear strength, C_u , of 50, 75 and
 337 100kPa. One dual-layered clay was studied, with a top layer of 50kPa over another layer
 338 of 75kPa. The embedded length of the pile, L , ranges from 25 to 30m (with intervals of
 339 1m) in the case of $C_u = 50$ kPa. All the conducted simulations are summarised in Table 9.
 340 The detailed input parameters of the models can be seen in the Methodology section.

Table 9. Information on the dynamic models conducted study cyclic behaviour.

Model No.	Pile Diameter, D (m)	Embedded Pile Length, L (m)	Undrained Shear Strength, C_u (kPa)	Number of Cycles, N
1	5.00			
2	6.25	25	50	100
3	7.50			
4	5.00			
5	6.25	25	75	100
6	7.50			
7	5.00			
8	6.25	25	100	100
9	7.50			
10	5.00			
11	6.25	25	50 & 75	100
12	7.50			
13		26		
14		27		
15	5.00	28	50	100
16		29		
17		30		

341 4.1. Time history of the pile rotation

342 The pile rotation angle can be calculated as follows:

$$\theta = \sin^{-1}(\delta/0.75H) \times (180^\circ/\pi) \quad (3)$$

where ϑ is the pile rotation (in degrees), δ represents the horizontal pile head displacement of the head of the pile (obtained from the model), and H is the total pile length. The rotation point of the studied monopiles in clay was found at about 75% of the embedded depth; this is also consistent with previous research [20].

The time histories of the pile rotation for the 17 simulations are plotted in Figure 13. Figure 13 (a) shows this result for the 5m diameter pile at 25m of embedded depth in various types of clay. As expected, the pile rotation in softer clays (with lower values of C_u) is larger than for stiffer clays (larger C_u). From Figure 13 (a), (b) and (c), the dual-layered soil with 50kPa (on the top layer) and 75kPa (at the bottom layer) of undrained shear strength has an intermediate pile rotation compared with the pile rotation in the 50kPa and 75kPa soils. The same trend was also found for the 6.25 and 7.5m diameter piles, which are shown in Figure 13 (b) and (c) respectively.

From Figures 13 (a), (b) and (c), we can conclude that the pile rotation decreases as the pile diameter increases. Also, it has been found that the 5m diameter pile embedded in 50kPa clay with 25m of embedded depth yields unstable behaviour because the rotations do not reach stable values, as in the other cases. From Figure 13 (d), after the embedded depth increases from 25 to 26m, the stability of the pile significantly improved. The pile rotation decreased when the embedded depth of the pile increased. Therefore, the increment of pile diameter and embedded depth can reduce the pile rotation and the stability of the pile can also be improved.

It is clear that unstable behaviour happened in the 5m diameter pile embedded in 50kPa clay with 25m of embedded depth. However, the monopile can also fail due to the accumulated rotation reaching a certain value after experiencing a high number of cycles, in the range of millions. This is away from the computation ability of the numerical simulation like the one presented in this paper. Therefore a procedure is required to predict the monopile rotation after any number of cycles. This procedure is derived and discussed in the following sections.

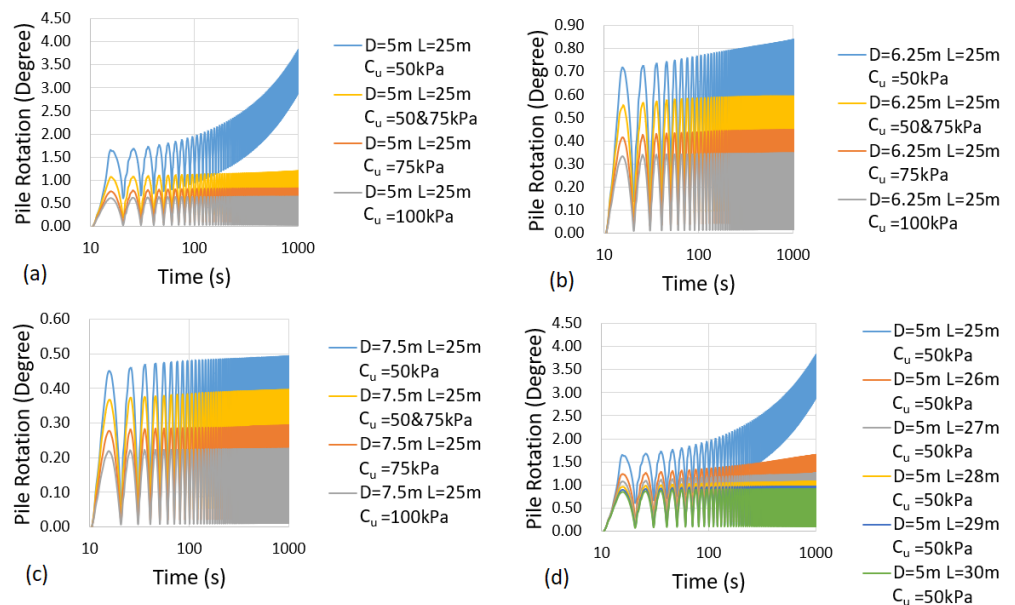


Figure 13. Time History of the rotation for the 17 simulations. (a) $D= 5\text{m}$, $L= 25\text{m}$. (b) $D= 6.25\text{m}$, $L=25\text{m}$. (c) $D= 7.5\text{m}$; $L=25\text{m}$. (d) $D=5\text{m}$, $L=\text{variable as shown}$.

4.2. Pile rotation in the first cycle

The pile rotations in the first cycle for the 17 simulations were extracted and summarized in Table 10. The accuracy of the pile rotations in the first cycle is mainly related to the monotonic performance of the numerical model, validated in many research studies

374 as well as in the current one. Therefore the accuracy of the pile rotations in the first cycle
 375 generated in this research can be assumed to be significantly high.

376 As discussed in the previous sections, the pile rotation is related to the pile diameter,
 377 embedded depth and undrained shear strength of the soil. Reducing the pile diameter
 378 and embedded depth results in increasing the pile rotation. The dual-layered soil
 379 with 50kPa and 75kPa of undrained shear strength has an intermediate pile rotation
 380 compared with those reached with the 50kPa and 75kPa soils. The average undrained
 381 shear strength (i.e. 62.5kPa) can be taken to represent the behaviour of the dual-layered
 382 soil. A significant linear relationship was found between the pile rotation in the first
 383 cycle in the logarithm scale and $D \times L \times \ln(C_u)$ in the natural logarithm scale (where D
 384 and L are given in meters and C_u in kPa). This relationship can be described using the
 385 following expression:

$$\theta_0 = 13.214 \times \exp\{-0.005 \times [D \times L \times \ln(C_u)]\} \quad (4)$$

386 where θ_0 represents the rotation in the first cycle (in degrees), and *exp* denotes exponen-
 387 tial.

388 In Figure 14, the value of $D \times L \times \ln(C_u)$ is plotted against the corresponding pile
 389 rotation in the first cycle for each simulation. This figure shows a strong correlation
 390 between both amounts, as previously mentioned, demonstrating a low uncertainty when
 391 Equation 4 is employed to predict the pile rotation in the first cycle.

392 In addition to the simulations conducted with horizontal load with amplitude of
 393 8MN, further analysis with 4 and 2MN have also been conducted. The maximum pile
 394 rotations in the first cyclic for these amplitudes are also presented in Figure 14, from
 395 which it can be concluded that these correlations are parallel one to each other in the
 396 range of $D \times L \times \ln(C_u)$ values explored. Initial rotations for other amplitudes (out of 8MN)
 397 can be obtained by interpolation, from the values presented in Figure 14. The regressions
 398 shown in Figure 14 can be generalised as:

$$\theta_0 = a \times \exp\{-b \times [D \times L \times \ln(C_u)]\} \quad (5)$$

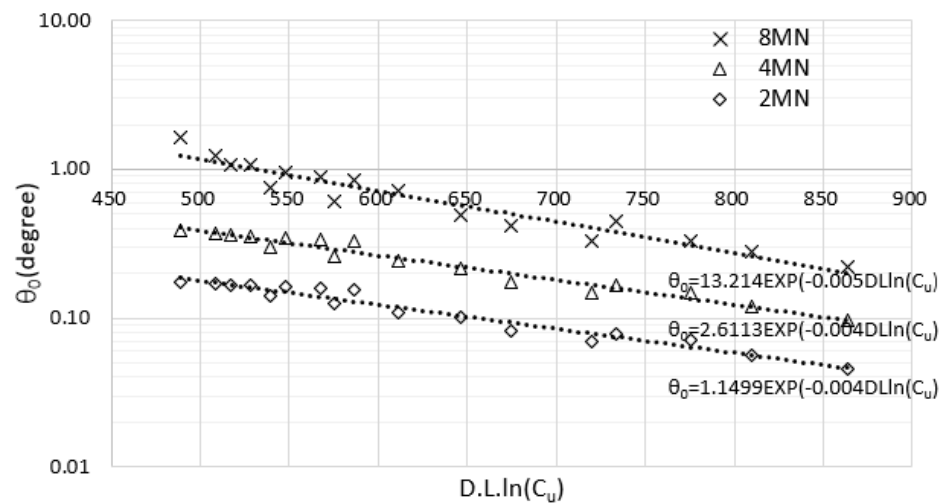
399 Since the regressions are roughly parallel one to each other, the constant b can be
 400 conservatively taken as 0.004. The constant a follows can be expressed as:

$$a = 0.5112 \times \exp(0.4067 \times F) \quad (6)$$

401 where F is the peak horizontal load (in MN).

Table 10. Pile rotations in the first cycle for the 17 simulations.

Model No.	Pile Diameter, D (m)	Embedded Pile Length, L (m)	Undrained Shear Strength, C_u (kPa)	D.L.ln(C_u) ($m^2 \ln(kPa)$)	Rotation ϑ_0 (degree)
1	5.00			489	1.65
2	6.25	25	50	611	0.72
3	7.50			734	0.45
4	5.00			540	0.76
5	6.25	25	75	675	0.42
6	7.50			810	0.28
7	5.00			576	0.61
8	6.25	25	100	720	0.33
9	7.50			863	0.22
10	5.00			517	1.07
11	6.25	25	62.5	646	0.49
12	7.50			775	0.33
13		26		509	1.24
14		27		528	1.08
15	5.00	28	50	548	0.96
16		29		567	0.89
17		30		587	0.85

**Figure 14.** Relationship between $D \times L \times \ln(C_u)$ and the corresponding pile rotation in the first cycle (agreement from Eq.4).

4.3. Cumulative rate of rotation

From the previous section, Equation 5 was developed to predict the initial pile rotation for the monopile with any given pile geometry embedded in clay with any undrained shear strength. The pile rotation in any given number of cycles can be correlated to the initial rotation, as justified hereinafter.

The cumulative rate of rotation is the ratio between the rotation in each cycle N , (ϑ_N), and the rotation in the first cycle (ϑ_0). The cumulative rate of rotation for each simulation has been plotted in Figure 15, from which we can see that, in most of the simulations, it follows a linear trend, in the logarithm scale, with the number of cycles, which is consistent with the findings given by other authors ([16],[11]). This indicates that the speed of the cumulative rate becomes lower as the number of cycles increases.

413 However, the tendency is significantly different in the case of a 5m diameter monopile
 414 embedded in 50kPa clay, with $L=25\text{m}$ ($D \times L \times \ln(C_u)=489$), 26m ($D \times L \times \ln(C_u)=509$) and
 415 27m ($D \times L \times \ln(C_u)=528$). This indicates that instability happens in these cases (i.e. when
 416 $D \times L \times \ln(C_u) < 528$). For these unstable monopiles, the pile diameter or the embedded
 417 depth should be increased to reduce the pile rotation.

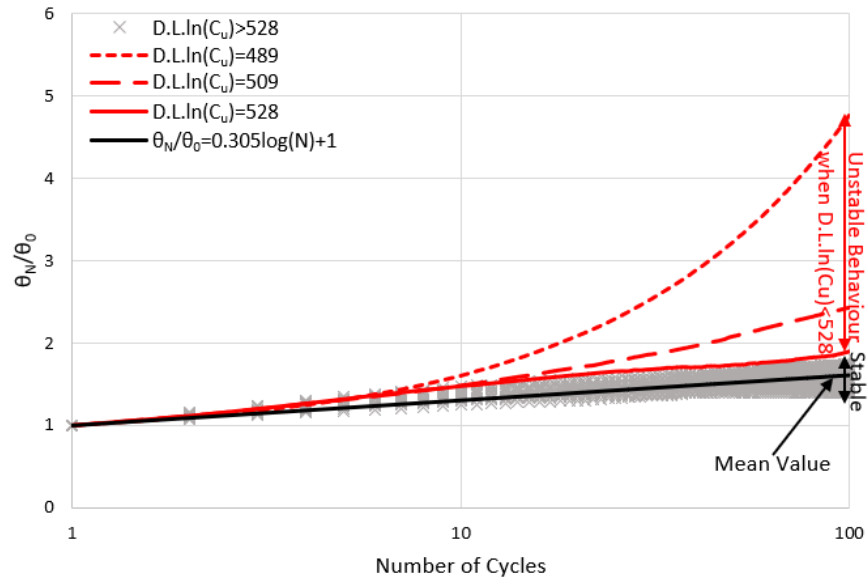


Figure 15. Cumulative rate of rotation for different values of $D \times L \times \ln(C_u)$.

418 The findings from the previous section can also be used to determine the stability of
 419 the monopile. The monopile behaviour becomes unstable when $D \times L \times \ln(C_u)$ is smaller
 420 than 528. Therefore, the stability can be immediately determined once the pile geometry
 421 and clay properties are available.

422 As in Figure 15, the cumulative rate for each simulation is very similar when the
 423 monopile reaches a point of stable behaviour (i.e. $D \times L \times \ln(C_u) > 528$). Therefore, the mean
 424 of the cumulative rate can be used to represent stable monopile cyclic behaviour. The
 425 mean of the cumulative rate can be described as:

$$\theta_N / \theta_0 = 0.305 \log(N) + 1 \quad (7)$$

426 For the case of 8MN of amplitude of loading (i.e. 5MW wind turbine), inserting
 427 Equation 4 into Equation 7 and rearranging, We can have:

$$\theta_N = 13.214 \times \exp\{-0.005 \times [D \times L \times \ln(C_u)]\} \times [0.305 \log(N) + 1] \quad (8)$$

428 Using Equation 8, the monopile rotation of a 5MW wind turbine in any load cycle
 429 can be determined.

430 When $D \times L \times \ln(C_u) < 528$, Equations 7 and 8 cannot be used, and the correspond-
 431 ing numerical simulation should always be conducted in such cases to determine the
 432 cumulative rate.

433 To conclude this section, the response of a monopile foundation under variable
 434 amplitudes of harmonic loading have been analysed. The geometry of this model is
 435 exactly same as the model with 7.5m diameter embedded 25m in 50kPa undrained shear
 436 strength of clay. The horizontal load applied can be described as

$$F(t) = \begin{cases} \text{abs}(2MN \times \sin(\pi t/10)), & 0s \leq t \leq 500s \\ \text{abs}(8MN \times \sin(\pi t/10)), & 500s \leq t \leq 1000s \\ \text{abs}(2MN \times \sin(\pi t/10)), & 1000s \leq t \leq 1500s \\ \text{abs}(8MN \times \sin(\pi t/10)), & 1500s \leq t \leq 2000s \end{cases} \quad (9)$$

437 A total of 200 cycles were applied to this model, with each cycle lasting 10s (0.1Hz).
 438 As it can be seen in Equation 9, the amplitude for the first 50 cycles was 2MN, 8MN for
 439 the next 50 cycles, 2MN for the following 50 and again 8MN for the last 50 cycles. The
 440 evolution of the rotation of the pile in time during this simulation is presented in Figure
 441 16, in comparison with the rotation obtained during 100 cycles of a constant amplitude
 442 of 8MN, plotted in two parts, jointly with the results for the two 50 stages (of 50 cycles
 443 each) of 8MN for the multi-amplitude loading. From this figure, it can be concluded
 444 that the rotation predicted in the case of load with variable amplitude is almost identical
 445 to the one achieved only for the number of cycles with higher amplitude (100 cycles of
 446 8MN). Therefore, it can be concluded that, in clayey soils, the effects of low amplitudes
 447 of loading is erased by higher loads. This is extremely relevant to save computational
 448 efforts in the simulations, as demonstrates that the loads with higher amplitudes (like
 449 those during storms) are those controlling the pile rotation, and the lower loads can
 450 therefore be neglected.

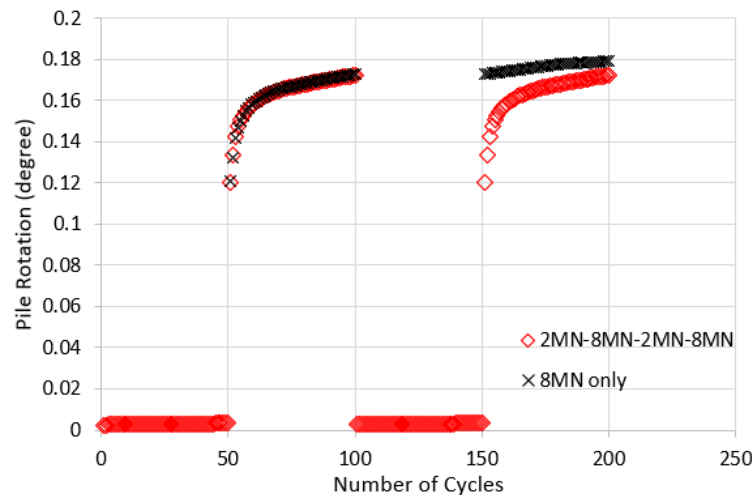


Figure 16. The cumulative rate of rotation for the single amplitude and multi-amplitude models.

451 Therefore, Equations 7 and 8 can be considered accurate enough, just applying the
 452 peak expected amplitude of load and the corresponding expected number of cycles for
 453 that amplitude.

454 5. Procedure to design monopiles in Clay

455 In order to improve the design procedures for offshore wind turbine monopile
 456 foundations in clay, a new procedure is presented in this paper, based on the previous
 457 findings. This new methodology can be described as follows:

- 458 1. determine the capacity of the offshore wind turbine; estimate the corresponding
 459 design horizontal load;
- 460 2. measure the undrained shear strength (C_u) of the clay in the seabed;
- 461 3. estimate the initial pile geometry that included the pile diameter (D) and the
 462 embedded depth (L);
- 463 4. calculate the pile wall thickness (through Equation 1);
- 464 5. calculate $D \times L \times \ln(C_u)$, and obtain the corresponding ϑ_0 from Figure 14 or Equation
 465 5;

- 466 6. estimate the number of storm cycles that the offshore wind turbine may experience;
 467 7. calculate the pile rotation under the number of storm cycles using Equation 7;
 468 8. if the rotation was larger than the design requirement, then we need to modify the
 469 dimensions of the pile and repeat the procedure from step 3.

470 It should be noticed that this design method was derived from the simulation results.
 471 The numerical simulations conducted in this research covered a monopile diameter range
 472 from 5m to 7.5m and undrained shear strength values for clays ranging between 50
 473 and 100kPa. Therefore, this design method is reliable for sizes and undrained shear
 474 strength within those ranges. For other values, the prediction may be unreliable. As
 475 previously discussed, the cyclic loads with higher amplitudes will erase the effect of
 476 those cycles with lower amplitudes. Hence, to design monopiles in clays, only the cycles
 477 under extreme loading conditions (i.e. storm events) that the offshore wind turbine will
 478 ever experience, have to be considered and explored. Equation 7 was derived based
 479 on the simulations undertaken for 8MN peak horizontal cyclic loads, representing a
 480 5MW offshore wind turbine. To design other types of wind turbine foundations with
 481 lower capacity (e.g. 3.5MW offshore wind turbine), Equation 7 is still conservative since
 482 a lower amplitude was investigated to have lower cumulative rate of rotation.

483 For a horizontal load of 8MN, if $D \times L \times \ln(C_u)$ is smaller than 528, then the monopile
 484 may have unstable behaviour. In such a case, it is recommended to conduct an accurate
 485 numerical simulation to predict the rotation. Conservatively, the pile diameter (D) or the
 486 embedded depth (H) can be increased and repeated as in step 3.

487 5.1. Design Example

488 5.1.1. 5MW Offshore Wind Turbine

489 In this example, the clay in the seabed is assumed to have 92kPa of undrained shear
 490 strength. The monopile employed to support 5MW offshore wind turbine was designed
 491 to have a diameter of 7m and 30m of embedded depth. The offshore wind turbine was
 492 predicted to experience 10 thousand large storms, each one with 100 cycles of horizontal
 493 loads with 8MN of amplitude of harmonic, one-way load. We first check if the pile
 494 behaviour will be in the stability range:

$$D \times L \times \ln(C_u) = 7 \times 30 \times \ln(92) = 950 > 528 \quad (10)$$

495 Therefore, the monopile is stable. The number of storm cycles is estimated as 10^6 ,
 496 and therefore, the pile rotation can be calculated as

$$\theta_N = 13.214 \times \exp\{(-0.005 \times [D \times L \times \ln(C_u)]) \times [0.305 \log(N) + 1]\} \quad (11)$$

$$\theta_N = 13.214 \times \exp\{(-0.005 \times [7 \times 30 \times \ln(92)]) \times [0.305 \log(1 \times 10^6) + 1]\} = 0.32^\circ \quad (12)$$

497 Thus, the expected maximum pile rotation after 1 million cycles of extreme horizon-
 498 tal loads is 0.32 degree for a 7m diameter monopile embedded 30m in 92kPa clay.

499 5.1.2. 3.5MW Offshore Wind Turbine

500 In this case, the seabed soil is assumed to be the same as in the previous case, with
 501 92kPa of undrained shear strength. The monopile used to support 3.5MW offshore
 502 wind turbine was designed to have a diameter of 5m and 30m of embedded depth. The
 503 weather conditions are also the same, with 10^6 of storm cycles, this time with 4MN of
 504 amplitude of horizontal load, as the turbine is smaller. From the regression equation
 505 shown in Figure 14, for 4MN peak horizontal load the maximum rotation in the first
 506 cycle can be calculated as

$$\theta_0 = 2.6113 \times \exp\{(-0.004 \times [D \times L \times \ln(C_u)])\} \quad (13)$$

$$\theta_0 = 2.6113 \times \exp\{(-0.004 \times [5 \times 30 \times \ln(92)])\} = 0.173^\circ \quad (14)$$

507 We can assume Equation 7 is conservative to estimate the cumulative rate of rotation
508 for 3.5MW offshore wind turbine monopile foundation. Therefore

$$\theta_N = [0.305 \log(N) + 1] \times \theta_0 = [0.305 \log(1 \times 10^6) + 1] \times 0.173 = 0.49^\circ \quad (15)$$

509 Therefore, the expected maximum pile rotation after 1 million cycles of extreme
510 horizontal loads is 0.49 degree for a 5m diameter monopile embedded in 92kPa clay
511 with 30m of embedded depth.

512 6. Conclusions

513 Monopiles can nowadays be considered as the most economic and reliable solution
514 for offshore wind turbine foundations. In the current design guidelines *p-y curves* are
515 derived for small diameter piles, as those used for gas platform foundations. Applying
516 the current design guidelines to offshore wind turbine monopile foundations might
517 generate an uneconomic solution.

518 In this research, the Mohr-Coulomb model was used to represent the undrained
519 behaviour of clay. Frictional contact was considered to describe the soil-pile interface.
520 Both monotonic and cyclic performances of the numerical model developed in this
521 research were successfully validated with reported centrifuge tests, demonstrating the
522 reliability of the adopted assumptions. The successful validations benefited from the
523 low uncertainty in the calibration of the Mohr-Coulomb model. For the undrained
524 scenario, only the undrained shear strength and the over-consolidation ratio require to
525 be measured during the experiments.

526 After the validation, a set of numerical models were conducted to investigate the
527 cyclic behaviour of monopiles with various geometries and different types of clay. The
528 time history of the pile rotation, for each simulation, was extracted and analysed. The
529 monopile rotation in clay is related to the pile diameter, the embedded depth and the
530 undrained shear strength of clay. After analysing the data, an empirical expression
531 to obtain the rotation for the first cycle of loading was obtained. In order to predict
532 the pile rotation at any cycle, the cumulative rate of rotation was determined. Similar
533 cumulative rates were found for monopiles displaying stable behaviour for increasing
534 number of cycles. However, for unstable monopiles, the cumulative rate was significantly
535 larger than the prediction. For the range of geometries and undrained shear strengths
536 simulated, the monopiles were found to be stable if $D \times L \times \ln(C_u)$ is larger than 528.

537 Finally, a new design procedure for offshore wind turbine monopile foundations
538 in clay has been presented. For any monopile diameter range from 5m to 7.5m and
539 undrained shear strength of clay range from 50 to 100kPa, the maximum pile rotation
540 in any cycle can be calculated using this procedure. Similar analyses can be conducted
541 for other geometries and clayey materials, to generalise the procedure presented in this
542 paper.

543 **Author Contributions:** Conceptualization and methodology, M.X. and S.L.; numerical models,
544 M.X.; writing—original draft preparation, M.X.; writing—review and editing, S.L.; data analyses
545 and visualization, M.X.; supervision, S.L. All authors have read and agreed to the published
546 version of the manuscript.

547 **Funding:** This research received no external funding.

548 **Institutional Review Board Statement:** Not applicable.

549 **Informed Consent Statement:** Not applicable.

550 **Data Availability Statement:** Not applicable.

551 **Conflicts of Interest:** The authors declare no conflict of interest.

552 **References**

- 553 1. HM Government *Meeting the Energy Challenge: A White Paper on Energy May 2007*; Department
554 of Trade and Industry: UK, 2007; pp. 7.
- 555 2. European Commission *The Paris Protocol A blueprint for tackling change beyond 2020*; Official
556 Journal of the European Union, 2015.
- 557 3. European Union *The European Council in 2014*; Publications Office of the European Union:
558 Luxembourg, 2015.
- 559 4. French, R.; Bonnett, D.; Sandon, J. Wind power: a major opportunity for the UK. *P I Civil
560 Eng-Civ En* **2005**, *158*, 20–27.
- 561 5. Carter, J.M.F. North Hoyle offshore wind farm: design and build. *P I Civil Eng-Energy* **2007**,
562 *160*, 21–29.
- 563 6. Abdel-Rahman, K.; Achmus, M. Finite element modelling of horizontally loaded monopile
564 foundations for offshore wind energy converters in Germany. In Proceedings of the interna-
565 tional symposium on frontiers in offshore geotechnics, ISFOG: Perth, Australia, 2005.
- 566 7. Moulas, D.; Shafiee, M.; Mehmanparast, A. Damage analysis of ship collisions with offshore
567 wind turbine foundations. *Ocean Eng* **2017**, *143*, 149–162.
- 568 8. DNV *Design of offshore wind turbine structures*; Det Norske Veritas: Norway, 2014.
- 569 9. Doherty, P.; Gavin, K.; Casey, B. The geotechnical challenges facing the offshore wind sector.
570 In *Geo-Frontiers 2011: Advances in Geotechnical Engineering*, Dallas, USA, 2011; Han, J.,
571 Alzamora, D.E., Eds.; American Society of Civil Engineers: Reston, USA, 2011.
- 572 10. Haiderali, A.; Nakashima, M.; Madabhushi, S. Cyclic lateral loading of monopiles for
573 offshore wind turbines. In *Frontiers in Offshore Geotechnics III*, 1st ed.; Meyer, V., Ed.; CRC
574 Press: Norway, 2015; pp. 711–716.
- 575 11. LeBlanc, C.; Houlsby, G.T.; Byrne, B.W. Response of stiff piles in sand to long term cyclic
576 lateral loading. *Geotechnique* **2010**, *60*, 79–90.
- 577 12. *API Geotechnical and foundation design considerations*; American Petroleum Institute: Washing-
578 ton DC, USA, 2011.
- 579 13. LeBlanc, C. Design of offshore wind turbine support structures: selected topics in the field of
580 geotechnical engineering. Ph.D. Thesis, Aalborg University, Denmark, 2009.
- 581 14. Jung, S.; Kim, S.R.; Patil, A.; Hung, L.C. Effect of monopile foundation modeling on the
582 structural response of a 5 MW offshore wind turbine tower. *Ocean Eng* **2015**, *109*, 479–488.
- 583 15. Thomas, S. *Geotechnical Investigation of UK Test Sites for the Foundations of Offshore Structures*;
584 The Stationery Office Books: London, UK, 1990.
- 585 16. Lau, B.H. Cyclic behaviour of monopile foundations for offshore wind farms. Ph.D. Thesis,
586 University of Cambridge, UK, 2015.
- 587 17. ANSYS, Inc. Ansys® Workbench, Release 18.0 Academic; 2016.
- 588 18. Lopez-Querol, S.; Cui, L.; Bhattacharya, S. Numerical methods for SSI analysis of offshore
589 wind turbine foundations. In *Wind Energy Engineering*, 1st ed.; Letcher, T.M., Ed.; Elsevier,
590 2017; pp. 275–297.
- 591 19. *USACE Engineering and design-settlement analysis*; U.S. Army Corps of Engineers: Washington
592 DC, USA, 1998.
- 593 20. Haiderali, A.; Madabhushi, G. Three-dimensional finite element modelling of monopiles for
594 offshore wind turbines. In *The 2012 world congress on advances in civil, environmental, and
595 materials research (ACEM 2012)*, Seoul, Korea, 2012; KAIST: Seoul, Korea, 2012.
- 596 21. Lehane, B.M.; Chow, F.C.; McCabe, B.A.; Jardine, R.J. Relationships between shaft capacity of
597 driven piles and CPT end resistance. *P I Civil Eng-Geotec* **2000**, *143*, 93–101.
- 598 22. Ramsey, N.; Jardine, R.; Lehane, B.; Ridley, A. A review of soil steel interface testing with
599 the ring shear apparatus. In Proceedings of the VI Conf. on offshore site investigation and
600 foundation behaviour; Society for Underwater Technology: London, UK, 1998.
- 601 23. Byrne, B.W.; Houlsby, G.T. Foundations for offshore wind turbines. *Philos T Roy Soc A* **2003**,
602 *2909*–2930.
- 603 24. Zhang, C.; White, D.; Randolph, M. Centrifuge modeling of the cyclic lateral response of a
604 rigid pile in soft clay. *J Geotech Geoenviron* **2010**, *137*, 717–729.
- 605 25. Hong, Y.; He, B.; Wang, L.Z.; Wang, Z.; Ng, C.W.W.; Masin, D. Cyclic lateral response and
606 failure mechanisms of semi rigid pile in soft clay: centrifuge tests and numerical modelling.
607 *Can Geotech J* **2017**, *54*, 806–824.